University of Baghdad
College of Engineering
JOURNAL OF ENGINEERING

Journal of Engineering

journal homepage: www.jcoeng.edu.iq

Volume 31 Number 6 June 2025

Crack Growth of Aluminum Alloy Sheets Used in Aircraft Wings, Taking into Consideration the Critical Angles of Attack

Shahad Nashat *, Fathi Alshamma

Department of Mechanical Engineering, College of Engineering, University of Baghdad, Baghdad, Iraq

ABSTRACT

This study examines the behavior of fatigue crack propagation in aluminum alloy sheets used in aircraft wings, with a particular focus on critical angles of attack (AOA). The widely utilized aluminum alloys 2024-T3 and 7075-T6 were analyzed to determine the effects of varying AOAs, representing normal flight (5°) and takeoff/landing (10°) on crack growth rates. A comprehensive approach was adopted, integrating experimental testing, numerical simulations, and analytical modeling. Experimental methods included material characterization and multiaxial fatigue tests using an innovative apparatus. Numerical simulations conducted with ANSYS 2021 CFD evaluated stress distributions and crack propagation under different wind loads and AOA conditions. Analytical modeling applied the Paris-Erdogan equation and fracture mechanics principles to predict crack growth behavior. The results revealed that higher AOAs significantly accelerate crack growth in both alloys. Notably, AL2024-T3 demonstrated slower crack propagation than AL7075-T6, indicating superior fatigue resistance, especially at lower AOAs. The fracture growth rates were determined to be 0.005 mm/sec for AL2024-T3 and 0.009 mm/sec for AL7075-T6. These findings have important implications for aircraft design, maintenance, and material selection. They underscore the necessity of accounting for AOA-dependent fatigue behavior to improve the durability and safety of aircraft structures.

Keywords: Computational Fluid Dynamics (CFD), Non-preoperational multi-axial cyclic loading, Angle of Attack (AOA).

1. INTRODUCTION

Modern aircraft, used for civilian and military transport, are engineering marvels composed of critical components, including the fuselage, engines, landing gear, tail assembly, and wings. The wings, integral to lift generation and stability, face significant challenges due to exposure to severe weather and unpredictable air disturbances. These disturbances result

*Corresponding author
Peer review under the responsibility of University of Baghdad.
https://doi.org/10.31026/j.eng.2025.06.09

Article received: 15/11/2024
Article revised: 30/12/2024
Article accepted: 21/01/2025
Article published: 01/06/2025

in fluctuating forces such as pressure, lift, and drag, which, when coupled with material flaws like voids, microcracks, and propagating cracks, can compromise the structural integrity of the wings, potentially leading to catastrophic failures **(Nalla et al., 2002; Sih and Wang, 2018; Liu and Xie, 2018; Harris and Smith, 2019).**

This research is necessary because the angle of attack (AOA) plays a critical role in influencing crack growth rates. AOA variations induce high stresses in wing structures, accelerating fatigue and crack propagation. Effective AOA management during flight and rigorous inspection of high-stress zones are essential strategies for mitigating these effects and ensuring the safety and durability of aircraft wings **(Rosenberg and Altus, 2020; Jensen et al., 2020).**

While previous studies have addressed general fatigue phenomena and crack growth under uniaxial loading, they often overlook the complex stress states induced by multiaxial loading conditions that better replicate real-world scenarios. This gap necessitates the development of advanced fatigue testing methods to evaluate the behavior of materials under combined cyclic loading, including pull-bending and torsion. Addressing this gap is particularly urgent for aluminum alloys like 2024-T3 and 7075-T6, widely used in aircraft structures, as they are highly susceptible to fatigue-induced failures under multiaxial cyclic loads **(Mustafa and Fathi, 2022; Hayder and Fathi, 2023).**

This study stands out for its comprehensive approach to analyzing fatigue crack growth in aircraft wings subjected to varying aerodynamic forces, particularly wind loads at different angles of attack (AOA). By integrating numerical simulations, theoretical modeling, and experimental methods, it offers valuable insights into crack propagation under both routine operational and extreme conditions. The emphasis on multiaxial fatigue testing introduces a novel perspective on the effects of proportional and nonproportional cyclic loading, addressing a significant gap in current research.

Fatigue crack propagation is a critical challenge in the aerospace industry, where aluminum alloys such as 2024-T3 and 7075-T6 are widely employed for their excellent strength-to-weight ratios. Despite their extensive use, the impact of AOAs on fatigue behavior remains underexplored. This research addresses this gap by investigating how critical AOAs influence crack growth in these alloys through a combination of experimental testing and computational analysis. The findings contribute valuable insights into the AOA-dependent fatigue behavior of aluminum alloys, with important implications for aircraft design, safety, and material optimization.

In summary, this study fulfills the need for a deeper understanding of multiaxial fatigue behavior in aluminum alloys, providing a new framework for evaluating structural integrity under complex aerodynamic loading conditions. These insights are crucial for advancing the development of safer and more durable aircraft structures, setting a foundation for future innovations in aeronautical engineering.

Figure 1. Piper PA-23-250 turbo **(Mark, 2014)**

2. NUMERICAL ANALYSIS

Numerical analysis is the branch of mathematics concerned with developing techniques for obtaining approximate solutions to mathematically formulated problems that cannot be solved exactly using analytical methods. These problems often arise in scientific computing, engineering, and other fields that rely heavily on mathematical models.
In this study, ANSYS CFD software is used to analyze airfoils. This software is highly effective for simulating airflow, making it a valuable tool for understanding the performance of wings and other lifting surfaces. These components are crucial for aircraft, as their design significantly impacts aerodynamic performance. CFD helps calculate lift, drag, pressure distribution, and center of pressure. The pressure distribution is then used to calculate equivalent (von Mises) stress and shear stress, which are essential to achieve the study's objectives **(Choudhury and Krishnamoorthy, 2018; Huang and Zhang, 2019).**
Finally, the powerful engineering simulation software ANSYS is used to obtain numerical results for da/dN (growth of crack per cycle) by entering Paris law parameters, including Paris law constants (c and m), as well as ΔK (change in stress intensity factor).

2.1. Computational Fluid Dynamics (CFD)

It is crucial in designing aerodynamically efficient airplanes and optimizing energy production. This branch of fluid mechanics leverages numerical analysis and data structures to simulate fluid flow, making it invaluable in various industries.
CFD is a powerful tool for simulating the flow of fluids around objects, including airfoils. Airfoils are wing-shaped structures used in airplanes, helicopters, and many other applications. The evaluation focuses on various angles of attack (α) **(Yuichi et al., 2010; Ahmed and Azhar, 2011).**
This study investigates the aerodynamic performance of a selected aircraft model using angles of attack of 5° and 10°. During cruise conditions, the angle of attack typically reaches a maximum of 5°, while for takeoff and landing, it increases to 10°. Maintaining an appropriate angle of attack is critical during landing, particularly during the flare maneuver near the runway. This ensures an accurate touchdown and prevents stalling, a potentially hazardous condition that necessitates immediate corrective action.
Using Computational Fluid Dynamics (CFD), engineers can evaluate the aerodynamic performance of an airfoil, including its lift, drag, and pressure distribution. Such insights are crucial for designing efficient and safe airfoils and studying phenomena like crack growth **(Setiawan, 2016).**
To accurately simulate wind pressure effects, a control volume **Fig. 2** was constructed, encompassing the air surrounding the wing model. In SOLIDWORKS, the wing volume was subtracted from the control volume to ensure realistic wind pressure interactions with all wing surfaces during the analysis.
A real wing model based on the Piper PA-23-250 Turbo aircraft's dimensions and specifications was utilized **(Mark, 2014).** The model was then imported into ANSYS Workbench for further analysis. Standard air properties were applied:

- Density: 1.3 kg/m^3,
- Temperature: 288.2 K,
- Viscosity: 1.8 × 10^{-5} kg·m/s.

An existing mesh with 5,257,573 tetrahedral elements and 1,480,229 nodes was used for the CFD simulation. The airflow entered the control volume at 117 m/s near the leading edge of the wingtip, while the outlet face was maintained at zero gauge pressure.
The CFD results provided detailed data on lift, drag, center of pressure, and the air pressure distribution on the wing surfaces, offering valuable insights into the aerodynamic characteristics **(Harsha et al., 2021).**

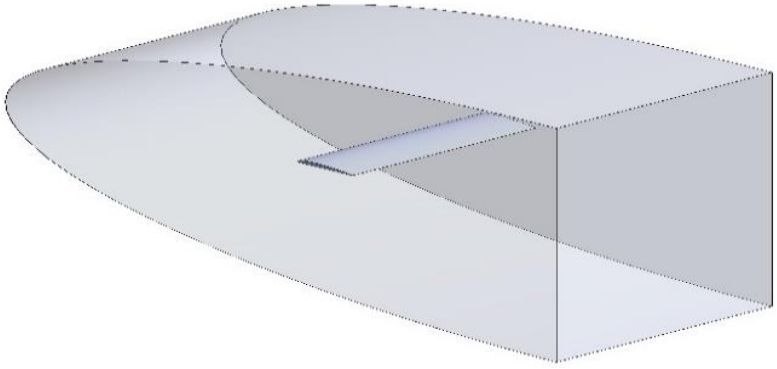

Figure 2. Geometry of CFD analysis.

The CFD pressure data informed the subsequent static structural analysis in ANSYS of a simplified cantilever wing model under fluctuating wind loads, analyzing stress variations across the structure through two separate simulations. Table 1 shows the material properties corresponding to the aluminum alloy **(Mallinson, 1999; Karima, 2012; Nasser and Mostaghimi, 2019).**

Table 1. Material properties of aluminum alloy **(Levent, 2010).**

No.	Material of aluminum alloy	
1	Density	2780 kg/m^3
2	Coefficient of Thermal Expansion	2.3×10^{-05} / ^{o}C
3	Reference Temperature	21 ^{o}C
4	Young's Modulus	73 GPa
5	Poisson's Ratio	0.33
6	Bulk Modulus	71 GPa
7	Shear Modulus	28 GPa
8	Tensile Yield Strength	385 Mpa
9	Compressive Yield Strength	385 Mpa
10	Tensile Ultimate Strength	483 Mpa

The computer model was divided into 5,257,637 tiny pyramid-shaped pieces called tetrahedra, which are part of the ANSYS software library, to understand how stress is distributed within the structure of the wings. The pressure distribution obtained from a separate fluid flow analysis was then applied, allowing the calculation of the lifting and pulling forces acting on the wing surface. These forces were incorporated into the meshed model. Finally, several key stress indicators, important to this study, are presented in **Table 2,** including the equivalent Von Mises stress in **Fig. 3** and the maximum shear stress in **Fig. 4**.

Table 2. Stress parameters for all multiaxial fatigue tests.

Stress	AOA 5^0	AOA 10^0
$\sigma_{Von-Mises}$	26.533 MPa	39.776 Mpa
τ_{max}	14.999 MPa	22.46 Mpa

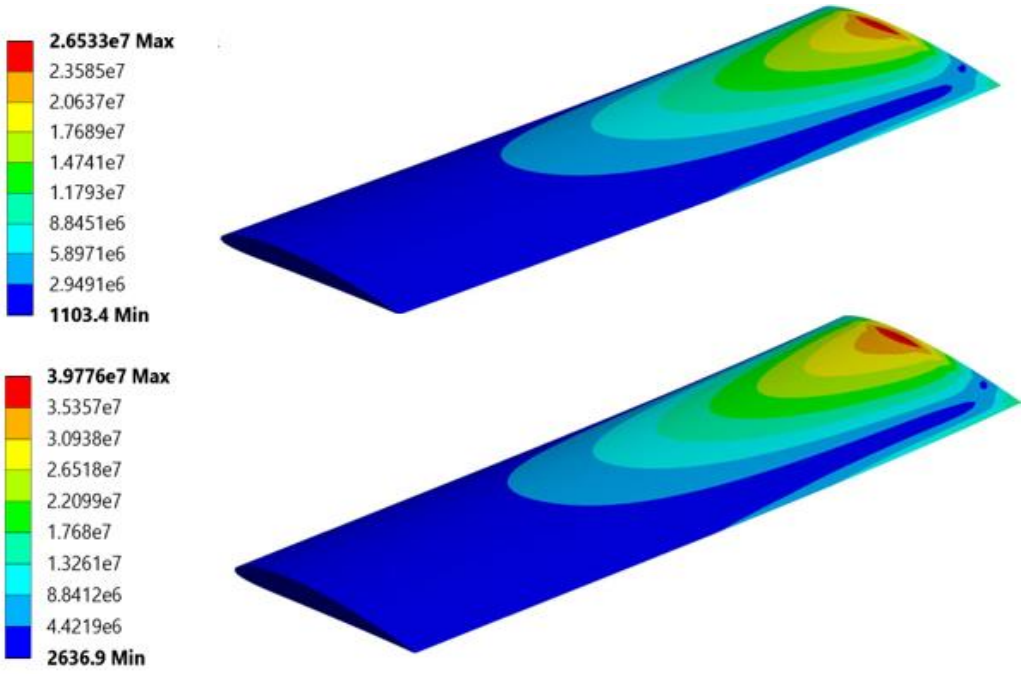

Figure 3. Equivalent stress (von Mises) at 5° and 10°.

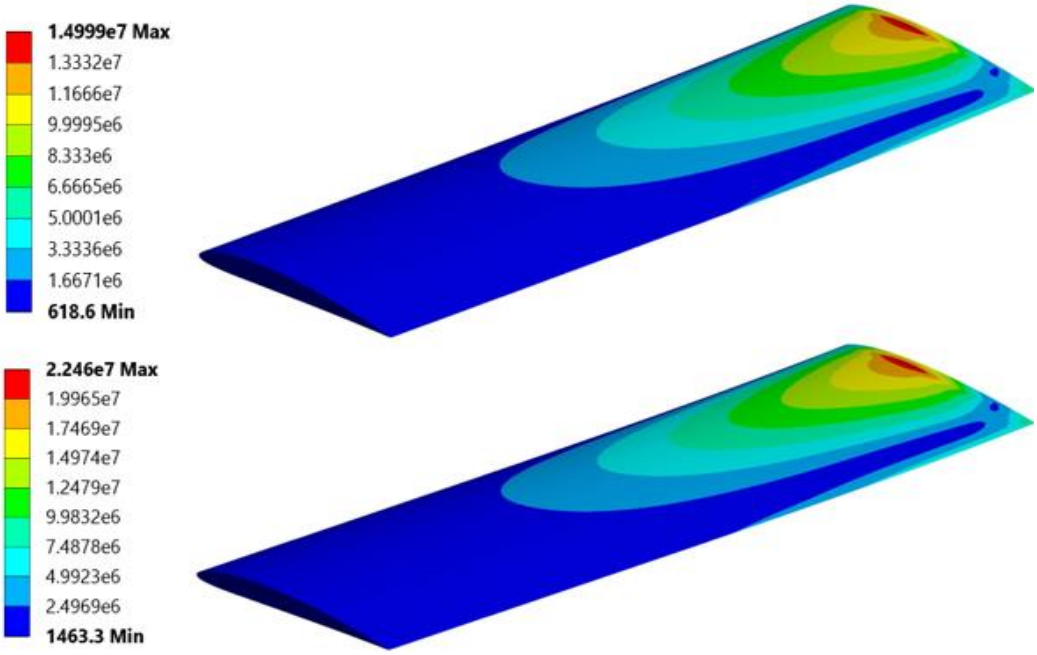

Figure 4. Maximum shear stress at 5^0 and 10°.

3. THEORETICAL ANALYSIS

This section explains how cracks spread under repeated loads from different directions (multiaxial cyclic loading). The study focuses on the lower surface of an airfoil made of aluminum alloy. A crack, 5 mm long, is created using a wire-cut machine. The plate used is 300 mm long, 60 mm wide, and 2 mm thick. The crack is placed 20 mm away from the leading edge, where shear stress occurs, see **Fig. 5.**

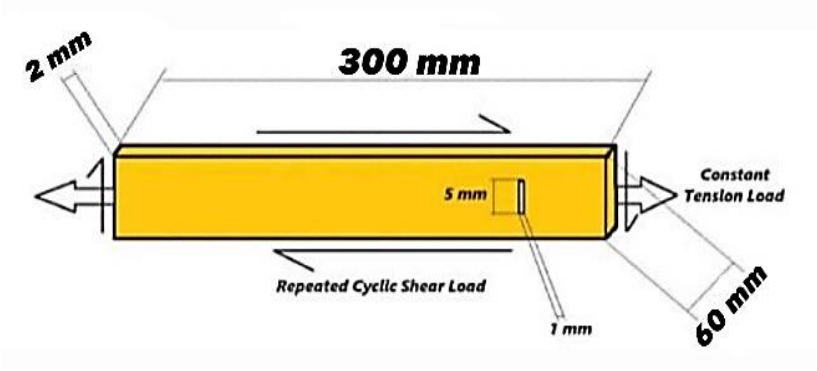

Figure 5. Multiaxial cyclic loading with the thin plate.

This study has explored a concept called the Griffith energy criterion. This criterion examines how energy behaves in a brittle material like aluminum alloy; this has been applied load on a flat plate of this material containing a single sharp crack running through it, see **Fig. 6.**

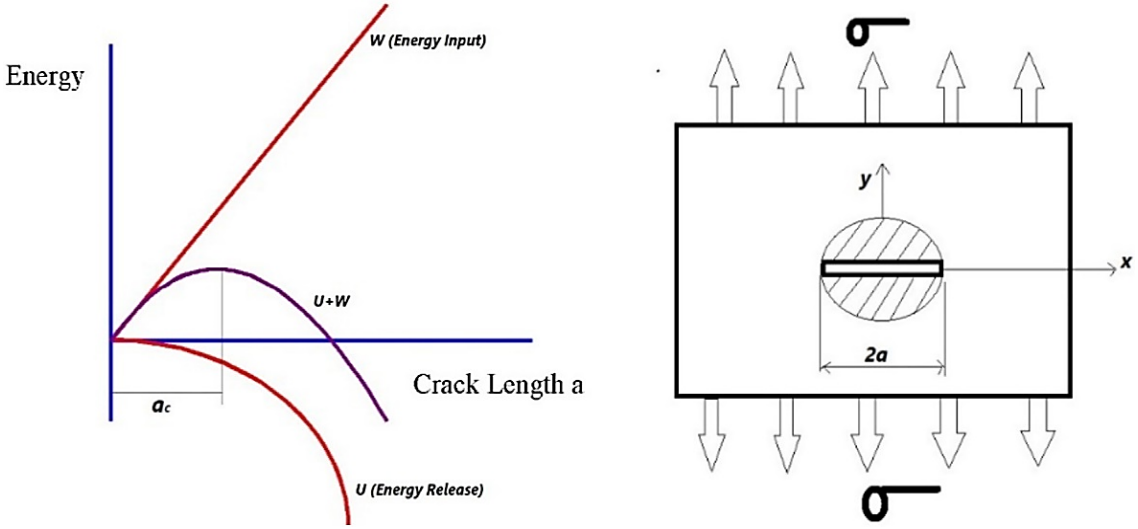

Figure 6. The relationship between energy input and release as a function of crack length. A material under constant pressure (σ) and experiencing repeated twisting forces (τ). **(Blazic et al., 2014)**

This creates a specific amount of stored energy per unit volume. This energy can be calculated using the following equation **(Blazic et al., 2014).**

$$U_0 = \frac{1}{2}\left(\sigma_X \varepsilon_X + \sigma_y \varepsilon_y + \sigma_z \varepsilon_z + \tau_{Xy}\gamma_{Xy} + \tau_{yz}\gamma_{yz} + \tau_{Xz}\gamma_{Xz}\right) \quad (1)$$

$$U_0 = \frac{1}{2E}\left(\sigma_X + \sigma_y + \sigma_z\right)^2 - \frac{2(1-\nu)}{E}\left(\sigma_X\sigma_y + \sigma_y\,\sigma_z + \sigma_z\sigma_x - \left(\tau_{Xy}{}^2 + \tau_{yz}{}^2 + \tau_{Xz}{}^2\right)\right) \quad (2)$$

$$U_0 = \frac{\sigma^2}{2E} + \frac{2(1+v)}{E}\left(\tau\ sin\left(\frac{\omega t}{2}\right)\right)^2 \quad (3)$$

$$U_0 = \left(\frac{\sigma^2}{2E} + \frac{2(1+v)}{E}\left(\tau\ sin\left(\frac{\omega t}{2}\right)\right)^2\right)\left(\pi a^2 \times \frac{h}{h}\right) = \left(\frac{\sigma^2}{2E} + \frac{2(1+v)}{E}\left(\tau\ sin\left(\frac{\omega t}{2}\right)\right)^2\right)\pi a^2 \quad (4)$$

1- The equation for the energy released per unit thickness is:

$$Delta\frac{\delta U}{\delta a} = \frac{\delta W}{\delta a} \quad (5)$$

2- Fracture occurs when the energy release rate reaches its maximum value **(Blazic et al., 2014):**

$$G = \frac{\partial U}{\partial a} = \left(\frac{\sigma^2}{2E} + \frac{2(1+v)}{E}\left(\tau\ \sin\left(\frac{\omega t}{2}\right)\right)^2\right)\frac{\pi a^2}{2} \quad (6)$$

The excess energy resulting from an unstable fracture can be written as **(Meggiolaro et al., 2005).**

$$U_e = \int_{a_0}^{a_i}(G - R)\,da \quad (7)$$

$$= -R\,(a_i - a_0) + \int_{a_0}^{a_i}\left(\frac{\sigma^2}{2E} + \frac{2(1+v)}{E}\left(\tau\ \sin\left(\frac{\omega t}{2}\right)\right)^2\right)\frac{\pi a}{2}da \quad (8)$$

$$\text{For R}=\left(\frac{\sigma^2}{2E} + \frac{2(1+v)}{E}\left(\tau\ \sin\left(\frac{\omega t}{2}\right)\right)^2\right)\frac{\pi a_i}{2} \quad (9)$$

Changing Eq. (5) into Eq. (4) yields **(Blazic et al., 2014):**

$$U_e = \left(\frac{\sigma^2}{2E} + \frac{2(1+v)}{E}\left(\tau\ \sin\left(\frac{\omega t}{2}\right)\right)^2\right)\frac{\pi a_0}{2(a_i - a_0)} + \frac{\left(\frac{\sigma^2}{2E} + \frac{2(1+v)}{E}\left(\tau\ \sin\left(\frac{\omega t}{2}\right)\right)^2\right)\pi}{4({a_i}^2 - {a_0}^2)} \quad (10)$$

$$U_e = \frac{\left(\frac{\sigma^2}{2E} + \frac{2(1+v)}{E}\left(\tau\ \sin\left(\frac{\omega t}{2}\right)\right)^2\right)\pi}{4({a_i}^2 - {a_0}^2)} \quad (11)$$

Engineers utilize a concept known as "effective stress" to calculate how much a crack spreads (kinetic opening displacement) in a thin plate under varied forces occurring in multiple directions (multiaxial loading). This reduces the complicated interaction of forces to a single, equivalent force acting in one direction. The equation below helps compute the effective stress **(Ragab and Salah, 1999).**

$$\sigma_{eff} = \frac{1}{\sqrt{2}}\sqrt{\sigma^2 + \left(\tau\ \sin\left(\frac{\omega t}{2}\right)\right)^2} \quad (12)$$

The effective stress idea works effectively in circumstances where two types of forces act in multiple directions (nonproportional multiaxial stress). In this paper, one force (σ) is constant and acts similarly to push down on an object. The other force changes direction regularly (cycling stress, similar to τ). In this example, the effective stress allows us to estimate how far the break will open vertically. The following equation demonstrates this calculation **(Ragab and Salah, 1999).**

$$V = \frac{2\sigma_{eff}}{E}\sqrt{a^2 - x^2} \quad (13)$$

Given that x is a function of (a), x = Ca can be expressed for 0 < C < 1 as follows **(Blazic et al., 2014)**

$$V = \frac{2\sigma_{eff}}{E}\sqrt{a^2(1 - C^2)} = C_1\frac{\sigma_{eff}\,a}{E} \quad (14)$$

Where $C_1 = 2\sqrt{(1 - C^2)}$

The displacement (v) will therefore change over time as the crack spreads and becomes:

$$Partial\ \frac{\partial V}{\partial t} = \frac{C_1}{E}\frac{\partial(\sigma_{eff}\, a)}{\partial t} \tag{15}$$

$$\frac{\partial V}{\partial t} = \frac{C_1}{E}\left(\frac{\partial \sigma_{eff}}{\partial t} a + \frac{\partial a}{\partial t}\,\sigma_{eff}\right) \tag{16}$$

$$\frac{\partial \sigma_{eff}}{\partial t} = \partial \frac{\left(\frac{1}{\sqrt{2}}\sqrt{\sigma^2 + \left(\left(\tau\,\sin\left(\frac{\omega t}{2}\right)\right)^2\right)}\right)}{\partial t} \tag{17}$$

$$\frac{\partial V}{\partial t} = \frac{1}{\sqrt{2}}\left(\sigma^2 + \left(\tau\,\sin\left(\frac{\omega t}{2}\right)\right)^2\right)^{-\frac{1}{2}} \tau^2 \omega\,\sin\left(\frac{\omega t}{2}\right)\cos\left(\frac{\omega t}{2}\right) \tag{18}$$

$$\frac{\partial V}{\partial t} = \frac{\omega \tau^2 \sin \omega t}{2\sqrt{2}\sqrt{\sigma^2 + \left(\tau\,\sin\left(\frac{\omega t}{2}\right)\right)^2}} \tag{19}$$

The kinetic energy of the crack displacement can be determined from the dynamic conditions for the crack growth **(Blazic et al., 2014):**

$$T = \frac{1}{2}\,\rho * Area * V^{0\,2} \tag{20}$$

$$T = \frac{1}{2}\,\rho \int\int \left(\frac{\partial V}{\partial t}\right)^2 dxdy \tag{21}$$

$$T = \frac{1}{2}\,\rho \frac{1}{E^2}\left[\left(\frac{\omega \tau^2 \sin \omega t}{2\sqrt{2}\sqrt{\sigma^2 + \left(\tau\,\sin\left(\frac{\omega t}{2}\right)\right)^2}} a\right) + \left(\frac{\partial a}{\partial t}\frac{1}{\sqrt{2}}\sqrt{\sigma^2 + \left(\tau\,\sin\left(\frac{\omega t}{2}\right)\right)^2}\right)\right]^2 \int\int C_1{}^2\, dxdy \tag{22}$$

The integral of $C_1{}^2$ in a semi-infinite plate is determined to be equal to ka^2, hence, Eq. (22) could be expressed as **(Blazic et al., 2014).**

$$T = ka^2\,\frac{1}{2}\,\rho \frac{1}{E^2}\left[\left(\frac{\omega \tau^2 \sin \omega t}{2\sqrt{2}\sqrt{\sigma^2 + \left(\tau\,\sin\left(\frac{\omega t}{2}\right)\right)^2}} a\right) + \left(\frac{\partial a}{\partial t}\frac{1}{\sqrt{2}}\sqrt{\sigma^2 + \left(\tau\,\sin\left(\frac{\omega t}{2}\right)\right)^2}\right)\right]^2 \tag{23}$$

According to Equations (11) and (18), the critical value for the fracture length becomes unstable and starts to grow when the strain energy U_e qual or exceeds the kinetic energy T:

$$\frac{\left(\frac{\sigma^2}{2E} + \frac{2(1+v)}{E}\left(\tau\,\sin\left(\frac{\omega t}{2}\right)\right)^2\right)\pi}{4(a_i{}^2 - a_0{}^2)} = ka^2\,\frac{1}{2}\,\rho \frac{1}{E^2}\left[\left(\frac{\omega \tau^2 \sin \omega t}{2\sqrt{2}\sqrt{\sigma^2 + \left(\tau\,\sin\left(\frac{\omega t}{2}\right)\right)^2}} a\right) + \left(\frac{\partial a}{\partial t}\frac{1}{\sqrt{2}}\sqrt{\sigma^2 + \left(\tau\,\sin\left(\frac{\omega t}{2}\right)\right)^2}\right)\right]^2 \tag{24}$$

$$= ka_i^2 \frac{1}{2} \rho \frac{1}{E^2} \left[\left(\frac{\omega\tau^2 \sin \omega t}{2\sqrt{2}\sqrt{\sigma^2 + \left(\tau \sin\left(\frac{\omega t}{2}\right)\right)^2}} a_i \right) + \left(\frac{\partial a}{\partial t} \frac{1}{\sqrt{2}} \sqrt{\sigma^2 + \left(\tau \sin\left(\frac{\omega t}{2}\right)\right)^2} \right) \right]^2 \quad (25)$$

The length of the crack attained at the release of excess energy is denoted by (a_i). Through the use of a MATLAB program and the Newton-Raphson method, it is possible to determine the velocity of crack growth $\frac{\partial a}{\partial t}$, for each time it takes to attain the crack length a_i, based on Eq. (25). Furthermore, it is discovered that the limit value $\frac{\pi}{k}$ for the case where $a_i >> a_0$ is smaller than unity. The major stresses for the component of the nonproportional multiaxial cycle loading can be computed as follows to verify the theoretical results **(Blazic et al., 2014):**

$$\sigma_{1.2} = \frac{\sigma_x + \sigma_y}{2} \pm \sqrt{\left(\frac{\sigma_x - \sigma_y}{2}\right)^2 + \tau_{xy}^2} \quad (26)$$

In this study's instance, since in points can be expressed as follows:

$$\sigma_{1.2} = \frac{\sigma}{2} \pm \sqrt{\left(\frac{\sigma}{2}\right)^2 + \left(\tau_{xy}^2 \sin\left(\frac{\omega t}{2}\right)\right)^2} \quad (27)$$

The following represents the angle at which the plane of major stresses will intersect the horizontal axis:

$$\tan 2\theta_p = \frac{2\tau_{xy}}{\sigma_x - \sigma_y} \quad (28)$$

Which, in the context of our case study, can be expressed as follows **(Ragab and Salah, 1999):**

$$\tan 2\theta_p = \frac{2\left(\tau_{xy} \sin\left(\frac{\omega t}{2}\right)\right)}{\sigma} \quad (29)$$

It is evident from Eq. (29) that the value of ωt will affect the angle at which the primary plane slopes toward the horizontal axis.

Given that the y-axis reflects the orientation of the fracture in the plate, the angle θp can be used to depict how the crack is inclined to the major stresses, the stress intensity factor can be expressed as follows: if $\sigma_2 = \alpha\sigma_1$, then σ_2 is always a compressive stress of the Moher circle for our investigation.

$$K_I = \frac{\sigma_1\sqrt{\pi a}}{2}\{(1+\alpha) + (1-\alpha)\cos 2\theta_p\} \quad (30)$$

$$K_{II} = \frac{\sigma_1\sqrt{\pi a}}{2}\{(1-\alpha)\sin 2\theta_p\} \quad (31)$$

Then $K_I = K_{Imax} - K_{Imin}$ where K_{Imax} is depend on the value of σ_{1max} when sin ωt = 1 and σ_{1min} when sin ωt = 0 AlsoK_{II} is depend on σ_{1max} and σ_{1min} then the mixed mode of I and II gives **(Blazic et al., 2014).**

$$\Delta K_{eq} = [\![\Delta K_I^4 + 8\Delta K_{II}^4]\!]^{0.25} \quad (32)$$

The growth of a crack can be calculated using the Paris law:

$$\frac{\partial a}{\partial N} = C(\Delta K_{eq})^{m} \quad (33)$$

m and c were determined for the current loading by graphing the log $\frac{\partial a}{\partial N}$ against log ΔKeq. The slope of the line indicates that m and C can be calculated from the junction of the line with the log $\frac{\partial a}{\partial N}$. $\frac{\partial a}{\partial N}$ was measured experimentally. The value of C, m, can be found in the linear zone using the following equation. Applying the equation:

$$\text{Log}\left(\frac{\partial a}{\partial N}\right) = m \log(\Delta K) + \log c \quad (34)$$

Furthermore, for confirmation, can derive the following theoretical formula for (θ_C) (Equations (36–37) from the corresponding sources **(Ewalds and Wanhill, 1989; Socie and Marquis, 2000; Richard et al., 2004).**

$$\theta_C = \pm\arccos\left[\frac{3K_{II}^{2}+K_I\sqrt{K_I^{2}+8K_{II}^{2}}}{K_I^{2}+9K_{II}^{2}}\right] \quad (35)$$

$$\theta_C = \tan{-1}\left[\frac{K_I}{4K_{II}} - \frac{1}{4}\sqrt{\left(\frac{K_I}{K_{II}}\right)^{2}+8}\right] \qquad K_{II} > 0 \quad (36)$$

$$\theta_C = \tan{-1}\left[\frac{K_I}{4K_{II}} + \frac{1}{4}\sqrt{\left(\frac{K_I}{K_{II}}\right)^{2}+8}\right] \qquad K_{II} < 0 \quad (37)$$

4. EXPERIMENTAL WORK

4.1 Wire Electrical Discharge Machining (WEDM)

It is a specialized technique for cutting intricate shapes in conductive materials, particularly metals. Unlike conventional cutting methods that use physical blades or mechanical forces, WEDM employs a thin, continuously fed wire electrode to generate electrical discharges, which erode and remove material from the workpiece. As shown in **Fig. 7**, WEDM was used in this study to cut all specimens for the various tests used in this study.

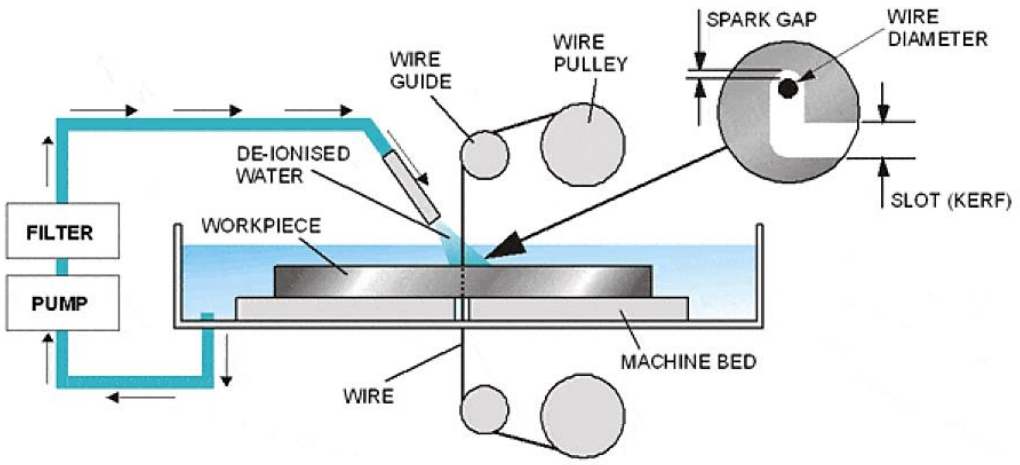

Figure 7. WEDM process flow schematic **(Tina et al., 2019)**

4.2 Tensile Test

The purpose of this test is to evaluate the mechanical properties of aluminum alloy specimens used in this study. As shown in **Fig. 8,** a rectangular specimen with dimensions of 250 mm in length, 30 mm in width, and 2 mm in thickness will be used. **Fig. 9** illustrates the tensile testing machine **(ASTM E8/E8M, 2020)**

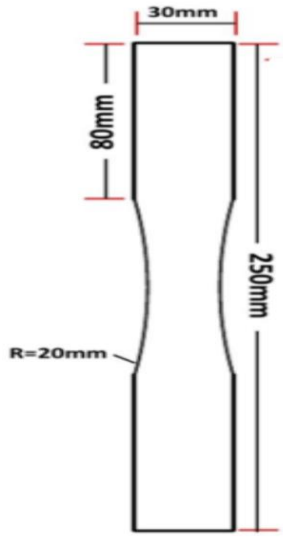

Figure 8. Tensile test specimen.

Figure 9. Tensile test machine.

Tables 3 and 4 show the material properties of two types of aluminum alloys.

Table 3. Material Properties of Alloy AL2024-T3.

No.	Material Alloy AL2024-T3	
1	Tensile Yield Strength	385 MPa
2	Compressive Yield Strength	385 Mpa
3	Tensile Ultimate Strength	483 Mpa

Table 4. Material Properties of Alloy AL7075-T6.

No.	Material Alloy AL7075-T6	
1	Tensile Yield Strength	436 MPa
2	Compressive Yield Strength	436 Mpa
3	Tensile Ultimate Strength	534 Mpa

4.3 Chemical Test

As illustrated in **Fig. 10**, a square aluminum alloy specimen with 20 mm sides was prepared for chemical analysis. The chemical testing machine used for this analysis is shown in **Fig. 11**. The objective of this test is to determine the chemical composition of both aluminum alloys **(ASTM E1251, 2019)**

Figure 10. Chemical test specimen.

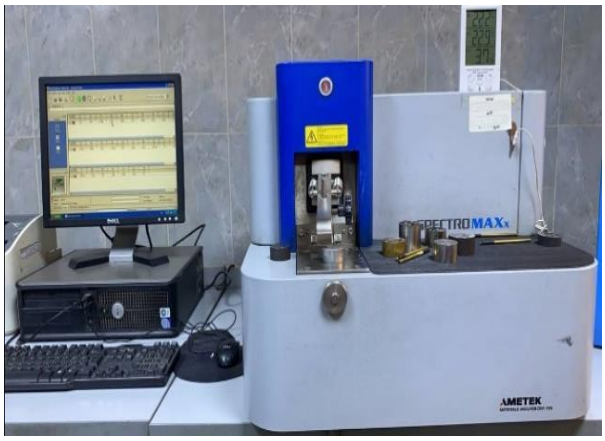

Figure 11. Chemical test machine.

Tables 5 and 6 show OES results for two types of aluminum alloys.

Table 5. OES Data for Alloy AL2024-T3.

Sample	Percentage	Sample	Percentage	Sample	Percentage
Si%	0.068	Mn%	0.346	Mg%	1.33
Fe%	0.243	Sn%	0.0044	Ni%	0.0069
Cu%	4.31	Al%	93.48	Zn%	0.0436
Ti%	0.0342	Pb%	0.0246	V%	0.0039

Table 6. OES Data for Alloy AL7075-T6.

Sample	Percentage	Sample	Percentage	Sample	Percentage
Si%	0.521	Mn%	20.37	Zn%	5.412
Fe%	0.534	Mg%	2.331	Ti%	0.314
Cu%	1.542	Cr%	0.354	Al%	89.86

4.4 Manufacturing of Multiaxial Fatigue Grip

A comparison was made between the experimental results obtained from a newly designed apparatus and the numerical results from ANSYS 2021 simulations, as well as theoretical solutions. This comparison focused on the growth behavior under constant tensile stress and cyclic in-plane shear stress, with tests conducted on four specimens. The stress levels varied according to the angle of attack (AOA) derived from CFD simulations. To ensure that crack growth remained within the linear elastic fracture mechanics (LEFM) range, a specific stress value was taken from CFD at AOA 5^0 and 10^0.

The study examined the rate of crack growth during the secondary stage for two types of alloys (AL2024-T3 and AL7075-T6) under two different stress conditions corresponding to AOAs of 5^0 and 10^0. Experimental results showed that the crack growth rate for aluminum alloys at 10^0 was 0.025 mm/s, while at 5^0 it was 0.013 mm/s. The crack growth behavior in thin plate specimens was analyzed in terms of the number of cycles at a 5^0 AOA and 10^0 AOA, and 10° AOA, crack growth indicated a greater resistance to crack propagation at a higher AOA in two types of alloys.

The study also evaluated crack initiation cycles, growth rates, and the effect of increased cycling on crack progression. It was observed that crack growth at 5° was slower despite a higher number of cycles, compared to 10^0 specimens in the two types of alloys.
Furthermore, crack kinking may occur in materials with anisotropic properties. Crack kinking can significantly affect the fatigue life of a material, as it creates a more complex crack path, making it harder to predict the remaining service life of a component. Therefore, the effects of nonproportional cyclic loading and crack kinking must be carefully considered when designing and analyzing structures subjected to cyclic loading, such as aircraft wings. **(Schijve, 2009; Anderson and Anderson, 2005; Omar and Fathi, 2019; Mustafa and Fathi, 2022).**
Fig. 12 shows a rectangular specimen of aluminum alloys representing the airfoil's lower surface with measurements of (300 mm X 60 mm X 2 mm), which was used and subjected to a multiaxial fatigue test.

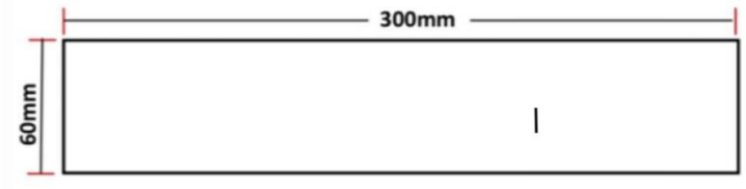

Figure 12. Fatigue test specimen.

Fig. 13 shows the multiaxial fatigue test rig, which is made from several main components, each with a critical role in delivering stress and monitoring crack propagation in the specimen.

Figure 13. Multiaxial fatigue rig.

Fatigue crack growth experiments were performed on two types of thin aluminum alloy plates subjected to multiaxial cyclic loadings. The tests were carried out on the maximum tension stress and the maximum shear stress in two cases at AOA 5^0 and 10^0. This paper used the linear elastic fracture mechanics regime to promote crack propagation using a frequency of 3 Hz and a load ratio (R) of zero.
This experiment, conducted using a newly developed apparatus, aimed to determine the constants (c and m) of the Paris-Erdogan equation within the linear elastic fracture mechanics framework. the values were C= ($3.6 \text{ X } 10^{-12}$) and m= (3.33).

This paper examined the spread of cracks in thin alloys (AL2024-T3 and AL7075-T6). An analysis of the propagation behavior of the fracture was conducted with an emphasis on the secondary phase of fracture expansion, which is marked by a constant growth rate. The experimental results showed that the crack growth velocity for AL7075-T6 was 0.009 mm/sec. For the AL2024-T3 alloy, the analytical crack growth velocity was 0.005 mm/sec.

5. RESULTS AND DISCUSSION

The results are presented in **Figs. 14-17**, illustrating the relationship between crack length and the number of cycles during multiaxial fatigue tests on AL7075-T6 and AL2024-T3 alloys at angles of attack (AOA) of 5° and 10°. Multiple AOA values were investigated as they significantly influence drag and lift forces, consequently impacting the ratio of shear stress to tensile stress and ultimately influencing crack propagation under non-proportional multiaxial fatigue conditions.

- AL2024-T3 at 5° AOA: The slowest crack propagation was observed in AL2024-T3 at 5° AOA, reaching approximately 11 mm after approximately 1,800,000 cycles. This indicates the highest resistance to crack growth in this condition, demonstrating the alloy's superior fatigue resistance at lower AOAs.
- AL2024-T3 at 10° AOA: A significant increase in crack propagation rate was observed in AL2024-T3 at 10° AOA, particularly after 240,000 cycles. While still exhibiting better fatigue resistance than AL7075-T6 at 10° AOA, this demonstrates the detrimental effect of higher AOAs on crack growth in this alloy.
- AL7075-T6 at 5° AOA: Crack propagation in AL7075-T6 at 5° AOA was observed to be slower than at 10° AOA, with steady progression over a larger number of cycles (up to around 760,000 cycles). This suggests that AL7075-T6 exhibits better fatigue resistance at lower AOAs.
- AL7075-T6 at 10° AOA: The most rapid crack growth was observed in AL7075-T6 at 10° AOA, with a significant acceleration after 169,000 cycles. This highlights the critical influence of high AOAs on crack growth in this alloy, indicating a higher susceptibility to fatigue failure.

5.1 Effect of Angle of Attack (AOA)

- A consistent trend across both alloys was observed: higher AOAs (10°) resulted in significantly faster crack growth than lower AOAs (5°). This is attributed to increased stress levels experienced by the wing structures at higher AOAs.
- These findings emphasize the critical role of AOA in influencing fatigue behavior and the need to consider AOA-dependent loading conditions in aircraft design and operation.

5.2 Limitations and Wider Applicability

- This study focused on two specific aluminum alloys and a simplified rectangular wing model. Further research is necessary to investigate the impact of AOA on a wider range of alloys and more complex wing geometries.
- The experimental setup, while replicating cyclic in-plane shear and constant tensile stress, may not fully capture the complex multiaxial loading conditions experienced by actual aircraft wings during flight.

- The findings of this study have significant implications for aircraft design and maintenance. By understanding the influence of AOA on fatigue crack growth, engineers can optimize the material selection, incorporate AOA-dependent safety factors in design, and develop more effective inspection and maintenance procedures to ensure continued airworthiness.

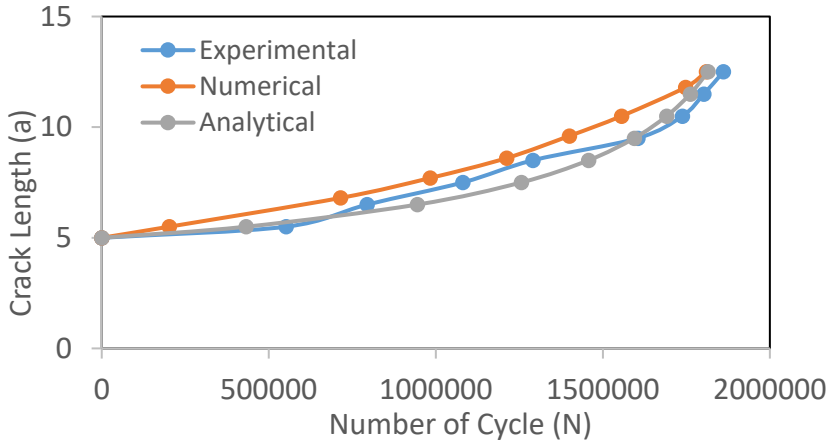

Figure 14. Crack length (mm) VS number of cycles (N) for AL 2024-T3 at AOA 5^0.

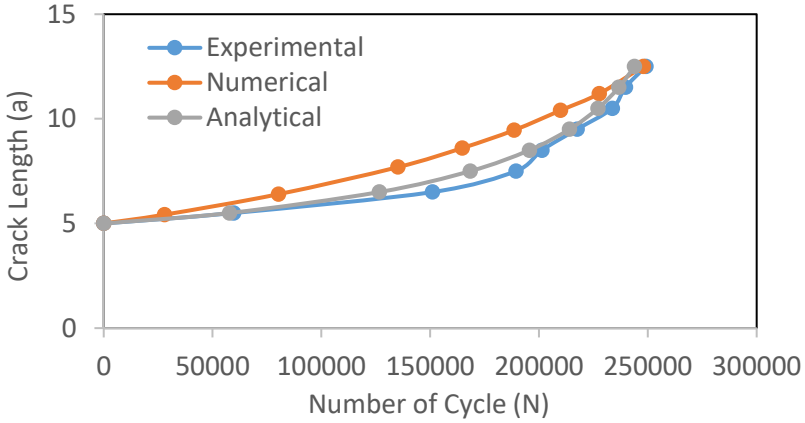

Figure 15. Crack length (mm) VS number of cycles (N) for AL 2024-T3 at AOA 10^0.

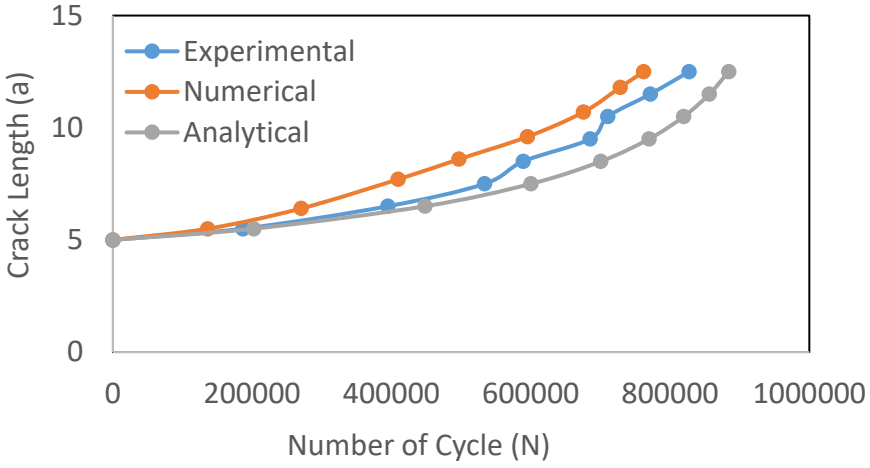

Figure 16. Crack length (mm) VS number of cycles (N) for AL7075-T6 at AOA 5^0.

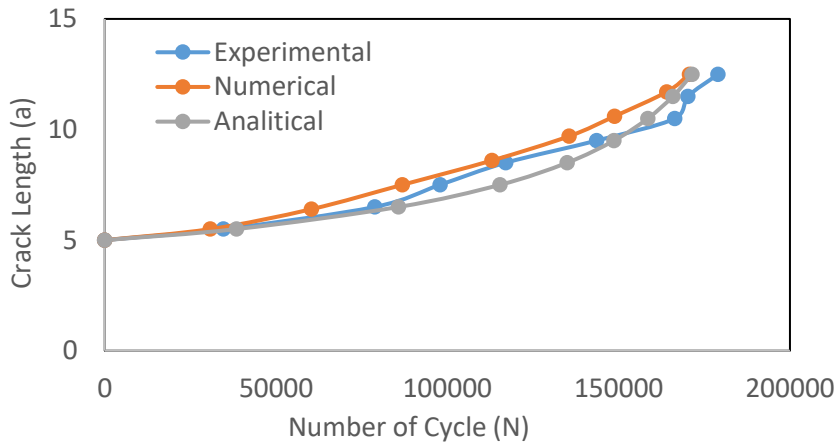

Figure 17. Crack length (mm) VS number of cycles (N) for AL7075-T6 at AOA 10^0.

Fig. 18, shows the stress ratio (τ/σ) influences crack propagation angles under multiaxial cyclic stress, with 30° angles ensuring slower propagation. Analysis using CFD and LEFM shows alloys (AL2024-T3, AL7075-T6) and variables like alloy type (e.g., AL6061) or angle of attack (e.g., 3°, 7°) can adjust (τ/σ), affecting crack behavior.

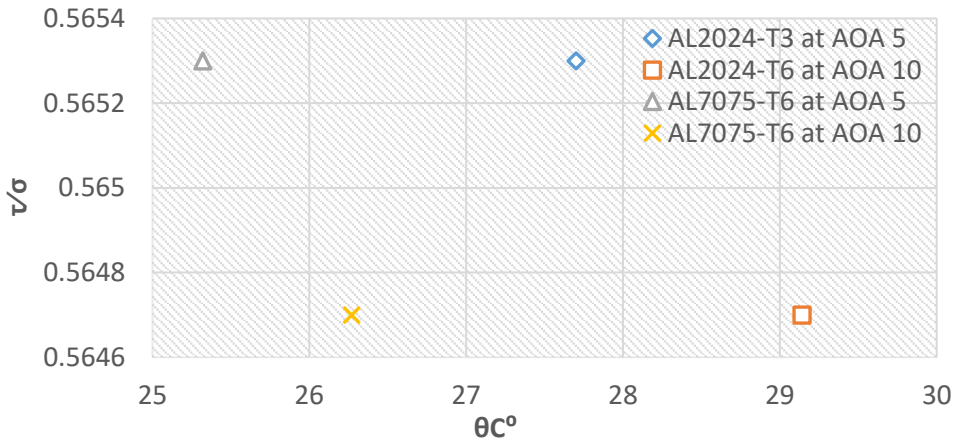

Figure 18. The Relation Between $(\frac{\tau}{\sigma})$ to The Angle of The Crack θ_c.

6. CONCLUSIONS

This study provides crucial insights into the influence of the angle of attack (AOA) on fatigue crack propagation in aircraft wings constructed from aluminum alloys. The results demonstrate a significant acceleration of crack growth at higher AOAs for both AL2024-T3 and AL7075-T6. Notably, AL2024-T3 exhibited superior fatigue resistance compared to AL7075-T6, particularly at lower AOAs. These findings underscore the critical need to consider AOA-dependent loading conditions in aircraft design, material selection, and operational procedures to enhance durability and safety. Future research should investigate the impact of AOA on a wider range of alloys and more complex wing geometries to further refine our understanding of fatigue behavior in aircraft structures.

NOMENCLATURE

Symbol	Description	Symbol	Description
a	Crack length, mm.	$K_{II\ max}$, $K_{II\ min}$	Maximum and minimum stress intensity factors in mode II (MPa$\sqrt{m}$).
a_i	Crack initiation, mm.	$K_{I\ max}$, $K_{I\ min}$	Maximum and minimum stress intensity factors in mode I, (MPa$\sqrt{m}$).
a_O	Original crack, mm.	m	The material constant found empirically from Paris law represents the value of (da/dN) at (dk=1 Mpa m), unit less.
N	Number of cycles.	R	Stress ratio = $(\sigma_{max})/(\sigma_{min})$, unit less.
U_e	Strain energy, J/m^3.	C	The material constant found empirically from the Paris law represents the interaction of slope with Y, m/(cycle $_X$ Mpa $_X$ m$^{1/2}$).
U_O	Energy stored per unit volume, Joule/m^3.	K_{eq}	Stress intensity factor in mode II, (MPa$\sqrt{m}$).
U	Energy released per unit thickness, Joule/m^3.	θ_P	The angle of the plane of the principal stresses, Deg.
da/dN	Crack growth per cycle, m/cycles	θ_C	The angle of crack direction, Deg.
ΔKeff	Effective stress intensity factor in mode I and II, (MPa$\sqrt{m}$).	σ_1	Maximum principal stress, MPa.
ρ	Density, Kg/m^3.	σ_{eff}	Effective stresses, MPa.
T	kinetic energy, Joule.	$\tau_{y.p}$	Yield shear stress of material, MPa.
ω	Angular frequency, radians per second.	σ_{min}, σ_{max}	Minimum and maximum applied shear stress, MPa.
K	Stress intensity factor (in mode I or mode II) in general (MPa).	K_{II}	Stress intensity factor in mode I, (MPa).
K_I	Plane strain resistance (MPa).	α	Angle of attack, Deg.

Credit Authorship Contribution Statement

Shahad N. Subhi: Writing –original draft, Methodology, Validation, manufacture of a new rig, Software, Conceptualization. Fathi A. AL-Shamma: Writing, review & editing.

Declaration of Competing Interest

The authors declare that they have no known competing financial interests or personal relationships that could have appeared to influence the work reported in this paper.

REFERENCES

Ahmed A. A., Azhar K. F., 2011. The static analysis of the composite aircraft wing box structure. *Journal of Engineering*, 17(06), pp. 1379–1390. https://doi.org/10.31026/j.eng.2011.06.06

Anderson, T.L. and Anderson, T.L., 2005. Fracture mechanics: fundamentals and applications. CRC Press.

ASTM E1251, 2019. Standard test method for analysis of aluminum and aluminum alloys by spark atomic emission spectrometry.

ASTM E8/E8M, 2020. Standard test methods for the testing of the tension of metallic materials.

Blazic, M., Maksimovic, S., Petrovic, Z., Vasovic, I., Turnic, D., 2014. Determination of the trajectory of fatigue crack growth and residual life under mixed modes. *Journal of Mechanical Engineering*, 60, pp. 250–254. https://doi.org/10.5545/sv-jme.2013.1354

Choudhury, D., Krishnamoorthy, V., 2018. CFD analysis of airfoil aerodynamics and stress distribution for the assessment of structural integrity. *Aerospace Science and Technology*, 79, pp. 400–410.

Ewalds, H. L., Wanhill, R. J. H., 1989. *Fracture Mechanics Handbook*. ISBN 0-7131-3515-8.

Harsha, P., Dazan, F., Arpit, K., Dhaneshwar, M., 2021. Finite element analysis of fatigue and fracture behavior in an idealized airplane wing model with an embedded crack under wind load. *Community-Based Research and Innovations in Civil Engineering*. https://doi.org/10.1088/1755-1315/796/1/012071.

Harris, D. S., Smith, T. L., 2019. Impact of aerodynamic loads and weather-induced forces on the integrity of the aircraft wings. *International Journal of Aerospace Engineering*, 7425412.

Hatem, R. W., 2016. Numerical and experimental analysis of aircraft wings subjected to fatigue loading. *Journal of Engineering*, 22(10), pp. 62–83. https://doi.org/10.31026/j.eng.2016.10.05

Hayder, K. S., 2016. The effect of vehicle body shapes on the near wake region and drag coefficient: a numerical study. *Journal of Engineering*, 22(9), pp. 115–131. https://doi.org/10.31026/j.eng.2016.09.08

Hayder, S. A., Fathi, A. Al., 2023. Propagation of dynamic crack growth of AL 2024 thin plates reinforced with carbon nanotubes subjected to nonproportional cycling loading. *Results in Engineering*, 19, 101239. https://doi.org/10.1016/j.rineng.2023.101239

Huang, Y., Zhang, L., 2019. Numerical analysis of airfoil aerodynamics using ANSYS Fluent for lift, drag, and pressure distribution. *Journal of Aerospace Engineering*, 32(3), 04019019. https://doi.org/10.1061/(ASCE)AS.1943-5525.0001006.

Jensen, C., Lee, H. J., 2020. Effect of the angle of attack on the growth of fatigue cracks in aircraft wings under aerodynamic loading. *Engineering Fracture Mechanics*, 228, 106934.

Karima, E. A., 2012. Experimental and numerical evaluation of the friction stir welding of AA 2024-W aluminum alloy. *Journal of Engineering*, 18(6), pp. 717-734. https://doi.org/10.31026/j.eng.2012.06.03

Levent, Ü., 2010. Structural design and analysis of mission-adaptive wings of an unmanned aerial vehicle. Thesis (MSc), Middle East Technical University, Turkey.

Liu, X., Xie, Y., 2018. Fatigue crack growth behavior of the aircraft wing structure under aerodynamic loads. *Journal of Aircraft*, 55(4), pp. 1254–1262.

Mallinson, G. D., 1999. Computational Fluid Dynamics Lecture Notes. *Department of Mechanical Engineering, University of Auckland*, Chapter 4, pp. 33–43.

Mark, K. Y., 2014. Piper-PA-23-250-Turbo-Aztec-F. *Aviation Photo*, #2398780. https://www.airliners.net/photo/Untitled/Piper-PA-23-250-Turbo-Aztec-F/2398780

Meggiolaro, M. A., Miranda, A.C. O., Castro, J. T. P., Marta, L. F., 2005. Stress intensity factor equations for the growth of branched cracks. *Engineering Fracture Mechanics*, 72, p. 2647–2671. https://doi.org/10.1016/j.engfracmech.2005.05.004

Mustafa, M. K., Fathi A. Al., 2022. Glass laminate aluminum reinforced epoxy under nonproportional multiaxial fatigue loading: experimental testing and new fatigue apparatus development. *Results in Engineering*, 16. https://doi.org/10.1016/j.rineng.2022.100773

Nalla, R. K., Campbell, J. P., Ritchie, R. O., 2002. Fatigue crack growth under variable-amplitude loading in aluminum alloys: Role of microstructure and environment. *Metallurgical and Materials Transactions A*, 33(2), pp. 283–293.

Nasser, A., Mostaghimi, J., 2019. *An introduction to computational fluid dynamics*. Chapter 20 of the *Fluid Flow Handbook*.

Omar, A. J., Fathi A. Al., 2019. Dynamic crack propagation in nanocomposite thin plates under multi-axial cyclic loading. *Journal of Materials Research and Technology*, 8, pp. 4672–4681. https://doi.org/10.1016/j.jmrt.2019.08.011

Rafid, M. M., Fathi, A. Al., 2022. Study the effect of multiaxial cycling loading on the dynamic crack propagation in aluminum plates. *International Journal of Mechanical Engineering*, 7(7).

Ragab, A. R., Salah, E. B., 1999. *Solid mechanics engineering.* CRC Press, ISBN 0-8493-1607-3.

Richard, H. A., Full, M., and Sander, M., 2004. Prediction of the crack path. *Institute of Applied Mechanics*, pp. 3–12. https://doi.org/10.1111/j.1460-2695.2004.00855.x.

Rosenberg, Z., Altus, E., 2020. Multiaxial fatigue of aluminum alloys under combined cyclic tension, bending, and torsion loading. *Fatigue and Fracture of Engineering Materials and Structures*, 43(10), pp. 2154–2166.

Schijve, J., 2009. *Fatigue of Structures and Materials*. Springer. https://doi.org/10.1007/978-1-4020-6808-9.

Setiawan, B., 2016. Simulation of the effect of airfoil NACA 4412 and MH60 with variations in the taper ratio on the C_L and C_D of unmanned aircraft for the surveillance mission. *Doctoral dissertation*, Gadjah Mada University, Jakarta.

Sih, G. C., Wang, Y., 2018. Fatigue behavior and testing of aluminum alloys for aircraft structures. *Materials Science and Engineering, A*, 710, pp. 251–261.

Socie, D. F., Marquis, G. B., 2000. *Multiaxial fatigue*. Warrendale, Pa: Handbook, Society of Automotive Engineers, ISBN 0-7680-0453-5.

Tina, C., Arindam, K. C., Arshad, N. S., Namrata, G., 2019. Effect of different dielectric fluids on material removal rate, surface roughness, kerf width, and microhardness. *The Brazilian Society of Mechanical Sciences and Engineering.* https://doi.org/10.1007/s40430-019-1845-1.

Yuichi, K., Kenji, T., Xin, Z., 2010. Computational investigation of a race car wing with vortex generators in ground effect. *Journal of Fluids Engineering*, 132, pp. 021102-1–021102-8. https://doi.org/10.1115/1.4000741

Zhao, W., Liu, X., 2017. Stress distribution and crack propagation in aircraft wings under variable loading conditions. *International Journal of Structural Integrity*, 8(2), pp. 193–204.

نمو الشقوق في صفائح سبائك الألمنيوم المستخدمة في أجنحة الطائرات مع مراعاة زوايا الهجوم الحرجة

شهد نشأت صبحي* ، فتحي عبد الصاحب الشماع

قسم الهندسة الميكانيكية ، كلية الهندسة الميكانيكية جامعة بغداد، بغداد، العراق

الخلاصة

تتناول هذه الدراسة سلوك انتشار شقوق التعب في صفائح الألمنيوم المستخدمة في أجنحة الطائرات، مع التركيز بشكل خاص على زوايا الهجوم الحرجة .(AOA) تم تحليل سبائك الألمنيوم الشائعة الاستخدام 2024 T3–و7075 T6–لتحديد تأثير زوايا الهجوم المختلفة التي تمثل ظروف الطيران العادي (5 درجات) والإقلاع/الهبوط (10 درجات) على معدلات نمو الشقوق.

تم اعتماد نهج شامل يتضمن الاختبارات التجريبية والمحاكاة العددية والنمذجة التحليلية. تضمنت الطرق التجريبية توصيف المواد واختبارات التعب متعددة المحاور باستخدام جهاز مبتكر. تم إجراء المحاكاة العددية باستخدام برنامج ANSYS 2021 CFD لتقييم توزيعات الإجهاد وانتشار الشقوق تحت أحمال الرياح المختلفة وظروف زوايا الهجوم. كما استُخدمت النمذجة التحليلية لتطبيق معادلة باريس–إردوغان ومبادئ ميكانيكا الكسر للتنبؤ بسلوك نمو الشقوق.

كشفت النتائج أن زوايا الهجوم الأعلى تُسرّع بشكل كبير من نمو الشقوق في كلتا السبيكتين. ولوحظ أن السبيكة AL2024–T3 أظهرت معدل نمو شقوق أبطأ مقارنةً بالسبيكةAL7075–T6 ، مما يشير إلى مقاومة أفضل للتعب، خاصة عند زوايا الهجوم المنخفضة. وقد تم تحديد معدلات نمو الشقوق بمقدار 0.005 ملم/ثانية للسبيكة AL2024–T3 و0.009 ملم/ثانية للسبيكة AL7075–T6.

تُبرز هذه النتائج أهمية كبيرة في تصميم الطائرات وصيانتها واختيار المواد. كما تؤكد على ضرورة أخذ تأثير سلوك التعب المرتبط بزوايا الهجوم في الحسبان لتحسين متانة وسلامة هياكل الطائرات.

الكلمات المفتاحية: ديناميكيات السوائل الحسابية، تحميل دوري متعدد المحاور غير متناسب، زاوية الهجوم.